https://doi.org/10.5194/egusphere-2022-798
Preprint. Discussion started: 31 August 2022

Elucidating the role of soil hydraulic properties on the aspect-dependent landslide initiation

Yanglin Guo[1, 2], Chao Ma[1, 2]

1. School of Soil and Water Conservation, Beijing Forestry University, Beijing 100083, PR China.
2. Jixian National Forest Ecosystem Observation and Research Station, CNERN, Beijing Forestry University, Beijing 100083, PR China.

Corresponding to: Professor Chao Ma, sanguoxumei@163.com

Abstract: Aspect-dependent landslide initiation is an interesting finding and previous studies merely address the role of plant roots on this observed connection between landslide probability and slope aspect. In this work, the aspect-dependent landslide initiation in catchment with same plant species and high vegetation coverage was examined by pore water pressure and hillslope hydrology behavior. Remote sensing interpretation using the high-resolution GeoEye-1 image and digitalized topography found that the landslides on south-facing slope have higher probability, larger basal area and shallower depth than those on north-facing slope. The lower limit of upslope contributing area and slope gradient condition for south-facing landslides is no less than north-facing landslides. The higher basal area of south-facing landslides over north-facing landslides may attribute to the high peak values and slow dissipation of pore water pressure. The absorbed and drained water flow in given time interval, together with the calculated water storage and leakage during the measured rainy season, sufficiently prove that the soil mass above the failure zone for the south-facing slopes are more prone to form pore-water pressure and result in slope failures. In comparison, the two stability fluctuation results from finite and infinite models imply that landslides on south-facing slopes may fail on condition of prolonged antecedent precipitation and intensive rainfall, while those on north-facing slopes may fail merely in response to intensive rainfall. The results of this work provide an insightful view on the aspect-dependent landslide initiation from both classical mechanics and the state of stress.

Keywords: Landslide; Pore pressure; suction stress; Hydraulic conductivity; Slope stability

1 Introduction

Shallow landslides are translational slope failures a few meters thick of soil mantle or regolith, and are destructive when they initiate or coalesce to form debris flows (Iverson et al., 1997; Wieczorek and Glade, 2005; Sidle and Ochiai, 2006). They may occur in wholly or partly in the unsaturated zone and enlarge their scale by the liquefaction mechanism (Godt et al., 2009). Understanding their occurrence can be broadly divided into two conceptual models, including the classical mechanics states that the failure surface is saturated and has compressive pore-water pressures acting on it (Reid et al., 1997; Lu and Godt, 2013), and the state of stress describes that the strength of soil and regolith is modified by infiltration and changes in soil matric suction (Lu and Likos, 2006).

The aspect-dependent landslides in Frontal Colorado, USA and the Loess Plateau, China have attracted interesting focus that vegetation generates a considerable influence on the landslide distribution. In fact, the overwhelming propensity for shallow landslide initiation on south-facing hillslope in the two regions closely relates to the present-day tree density, regardless of hillslope aspect (Ebel, 2013; Rengers et al., 2016; Deng et al., 2022). In the Colorado Frontal Range, field observations proved that south-facing slopes lack thick tree cover and have an abundance of rock outcrops compared to north-facing slopes, and the soil layer would be thinner on south-facing slopes (Smith et al., 2011; Coe et al., 2014; Ebel et al., 2015; Timilsina et al., 2021). The apparent cohesion supplied by roots was responsible for the observed connection between landslide distribution and slope aspect (McGuire et al., 2016). In the Loess Plateau China, vegetation recovery is the major ecological measure to mitigate the sediment loss (Zhou et al., 2006; Fu et al., 2009). Promoted soil strength and hydraulic conductivity due to strong root network may enhance the topographic initiation condition (Montgomery and Dietrich, 1994; Schmidt et al., 2001; Wang et

https://doi.org/10.5194/egusphere-2022-798
Preprint. Discussion started: 31 August 2022

al., 2020; Dai et al., 2022). Besides, the shallow landslide depth approximately increases with the plant roots depth and the vegetation coverage (Guo et al., 2020; Li et al., 2021). Another possibility is that the north- and west-ward moving storm produced more intense rainfall on south- and east facing slope. Such assumption may be invalid if aspect-dependent landslide distribution exists in a localized catchment with given vegetation communities. In fact, the above-mentioned study highlights the effect of mechanical function of plants on landslide. If the aspect-dependent landslide exists in a localized area with high vegetation and same plant species, the mechanical effect of plant roots would not be responsible for the observed connection.

Except the observed connection between vegetation and aspect-dependent landslide, the differences in landslide scale have been neglected. Indeed, aspect-dependent landslide distribution may result from soil strength property associated behavior, such as excessive pore water pressure dissipation and sliding surface liquefaction owing to undrained loading (Terzaghi, 1950; Sassa, 1984; Youd and Gilstrap, 1999), and the hillslope hydrology behavior including soil water storage capacity, drainage ability and the changes in matrix suction (Godt et al., 2009; Geroy et al., 2011; Yang et al., 2017; Thomas et al., 2018; Lee and Kim, 2019; Marino et al., 2021). When the slope fails, the pore water pressure abruptly increases within the shear zone (Brenner et al.,1985; Iverson and LaHusen, 1989; Wang and Sassa, 2003; Wang et al., 2003). If the excessive pore water pressure persists high over the static pressure for a long duration, the displaced masses will enlarge their volume by widespread liquefaction (Lan et al., 2003; Bogaard and Greco, 2016). In other words, the magnitude of the pore water pressure closely relates to the scale of the shallow landslide. Furthermore, some statistical results reveal that incoherent materials favor shallow landslides with no limitation in size; cohesive materials favor deep landslides and show a limitation for small sizes (Larsen et al., 2010; Frattini and Crosta, 2013; Milledge et al., 2014). Therefore, the scale of the shallow landslides could be elucidated by the role of excessive pore water pressure during the failure process. However, the aspect-dependent landslide distribution in the two above-mentioned areas merely refers to the differences in landslide probability, not the landslide scale.

Examining the aspect-dependent landslide distribution does not merely focus on the effect of moisture-related hydrology behavior on slope stability, but on the soil strength-associated behavior on the landslide scale. This work firstly documented the aspect-dependent landslide initiation and landslide scale in a localized area, Loess Plateau China. Then, the physical properties of soil mass and pore water pressure dissipation were compared with respect to the landslide scale. Finally, field volumetric water content (VWC) at varied soil layers were monitored to examine the water storage capacity and drainage ability, and the changes in suction stress and slope stability. The results of this work may provide insightful understanding of the aspect-dependent landslide distribution in some mountain areas of the Northern hemisphere.

2 Study area

The study area is in the mountain region near Niangjiangba town, Tianshui City, Gansu Province, Central China. It is also close to the dividing crest of the Yellow River and Yangtze River, and in the eastern part of the Loess Plateau. Though it is a small part of the Loess Plateau, the soil layer in the study area is no more than 3 m. Majority of the hillslope are underlain by slate; the stratigraphic units of granite, sandstone, and mudstone account for a relatively smaller area. This area in semi-humid climate region and has four distinctive seasons. The annual precipitation is approximately 491.6 mm and mostly falls during June and August. One branch fault of the Tianshui-Lanzhou fault system runs through the area and has no rupture records for the last few decades.

The shallow landslides in the whole area were triggered by the prolonged antecedent precipitation during 1 to 24 July and the intensive rainstorm on 25 July 2013 (Yu et al., 2014; Guo et al., 2015). Previous studies found that majority of shallow landslides have gradient of 20–25°, locate on south-facing slopes and in areas with sparse vegetation (Li et al., 2021). Besides, the strong root network may promote the hydraulic conductivity of soil-root

https://doi.org/10.5194/egusphere-2022-798
Preprint. Discussion started: 31 August 2022

composite and the landslide initiation condition of upslope contributing area-slope gradient (Dai et al., 2022). The selected study area in this work is in the central part and underlain by granite unit. The total area is 0.88 km^2 and contains three small catchments, with vegetation coverage rate of over 90% (Fig. 1). The relative relief is about 200 m and the mean hillslope gradient is 37 °. On the south- and north-facing slope in the three catchments, the main plant species is *Larix Kaemphferi*, which commonly have highly-developed lateral roots with depth < 0.4 m.

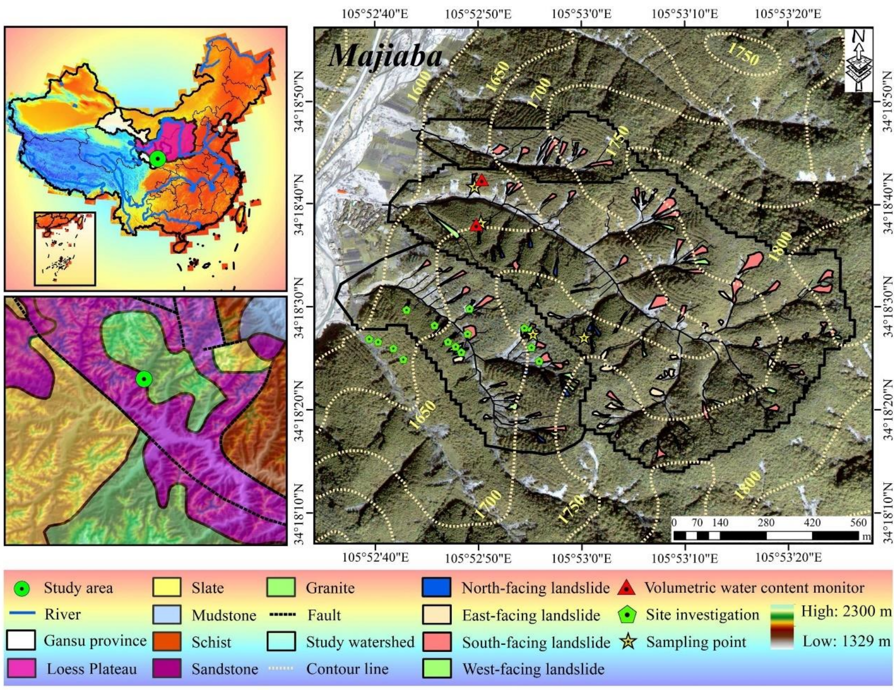

Fig. 1. Location, topography, and simplified lithology of the study area. (All maps are created by the authors. The graph of Majiaba was taken by an Unmanned Aerial Vehicle. The territorial domain of China and simplified lithology map are from China Geological survey)

3 Materials and methods

3.1 Landslide information interpretation

The high-resolution (0.5 m × 0.5 m, on October 8, 2013) GeoEye-1 image was orthorectified and the landslide boundary was visually interpreted by ENVI 5.1 and e-Cognition 8. An unmanned aerial vehicle (UAV for abbreviation) was used to obtain the digital elevation model (DEM) with 5 m resolution. The GeoEye-1 orthographic image and DEM were spatially registered in the ArcGIS 10.2 by standard layer of orthoimage. The landslide initiation condition is represented by the competition between slope gradient and the upslope contribution area (*A*-*S*):

$$S=kA^{-b} \tag{1}$$

where *S* is the local slope (m/m); *A* is the contribution area above landslide head-scar (m^2); *k* is an empirical constant, which is related to lithology, vegetation, and climate; *b* is an empirically defined index.

Field investigation mainly to measure the depth of head-scar and sidewall area by tape, and the failure depth is taken as the average of them. Then, the landslide volume can be calculated by the interpreted scar area and the measured depth. Finally, detailed landside information, including the landslide number and area probability, landslide volume and width, head-scar and sidewall depth, as well as the upslope contributing area-slope gradient

https://doi.org/10.5194/egusphere-2022-798
Preprint. Discussion started: 31 August 2022

condition for the south- and north-facing slope were compared.

3.2 Field monitoring and soil sampling

To investigate the hillslope hydrology on the south- and north-facing slope, the Frequency Domain Reflectometry (FDR) soil moisture sensors at three soil layers of 30cm, 70cm, and 110cm each slope was implemented to monitor the volumetric water content during the rainy season 2021. The meteorological station is no more than 3 km away from the study area to record the rainfall on 30 min basis. During the sensors implement, the undisturbed soil samplings near the sensor location were taken for indoor tests, including dry unit weight, porosity, grain size, and hydraulic conductivity. The grain size was analyzed by Malvern MS 3000 (Malvern, England). In each layer, at least 4 samples are collected for consolidated undrained triaxial compression test (CU), and 2 samples for unsaturated hydraulic conductivity measurement by transient release and imbibition method test (Lu and Godt, 2013). Saturated hydraulic conductivity was determined using constant water head method (Table 1)

3.3 Pore water pressure dissipation

We performed CU tests to obtain the effective cohesion, effective internal friction angle, and the pore pressure water dissipation curves. The soil sampling, with diameter 50 mm and height of 100 mm, were firstly saturated in a vacuum pump, then consolidated in the chamber of GDS apparatus by 50, 100, 150, and 200-kPa confining pressure and 10-kPa backpressure, and the shearing rate was 0.1 mm/min. During each CU test, the pore water pressure gradually increases to peak, then dissipate afterwards. Owing to the varied particle component and soil texture, the increasing and dissipation ratio varies. Furthermore, such ratio closely relates to the widespread generation of excessive pore water pressure, which will enlarge the landslide scale. High excessive pore water pressure, rapid increase ratio and slow dissipation ratio could cause widespread coulomb failure within the sliding zone. To show the pore water pressure increase or dissipate, the ratio is:

$$i = \frac{p_{t+\Delta t} - p_t}{\Delta t} \tag{2}$$

where i is the increase or dissipation ratio of excessive pore water pressure, p_t and $p_{t+\Delta t}$ are the measured pore water pressure during the time interval of Δt.

3.3 Water storage and drainage

The unsaturated permeability of soil mass (diameter 61.8mm, height 25.4mm) was measured by Transient Release and Imbibition method (TRIM) (Lu and Godt, 2013). In this test, the water outflow mass was measured on 10 minutes basis. In each test, the air pressures of 250 kPa and 0 kpa correspond to drying and wetting process respectively. Thus, the Soil Water Characteristic Curve (SWCC) and the Hydraulic Conductivity Function (HCF) would be obtained by the Hydrus 1-D (Wayllace and Lu, 2012). Using the models proposed by Mualem (1976) and van Genuchten (1980), the constitutive relations between suction head (h), water content (θ), and hydraulic conductivity (K) under drying and wetting state could be represented by following equation:

$$\frac{\theta - \theta_r}{\theta_s - \theta_r} = \left[\frac{1}{1 + (\alpha|h|)^n}\right]^{1-\frac{1}{n}} \tag{3}$$

and

$$K = K_s \frac{\left\{1 - (\alpha|h|)^{n-1}[1 + (\alpha|h|)^n]^{\frac{1}{n}-1}\right\}^2}{[1 + (\alpha|h|)^n]^{\frac{1}{2}-\frac{1}{2n}}} \tag{4}$$

where θ_r is the residual moisture content, %; θ_s is the saturated moisture content, %; α and n are empirical fitting parameters with α being the inverse of the air-entry pressure head and n the pore size distribution parameter; K_s is the saturated hydraulic conductivity, cm/s.

The soil water storage (S_s) and drainage (S_d) during a rainfall event can be evaluated by the soil depth and the difference between the maximum soil moisture and the antecedent soil moisture:

https://doi.org/10.5194/egusphere-2022-798
Preprint. Discussion started: 31 August 2022

$$S_e = \frac{\theta - \theta_r}{\theta_s - \theta_r} \tag{5}$$

$$S_s = S_e^w \Delta h \tag{6}$$

$$S_d = P - S_e^d \Delta h \tag{7}$$

where S_e is the saturation degree; θ is the measured volumetric moisture content, %; Δh is the average soil thickness, mm (400 mm in this work); S_e^w and S_e^d are the residual soil moisture in wetting and drying process, %; P is the accumulated rainfall, mm.

3.4 Stability fluctuation

In this work, we applied finite and infinite stability model to assess the slope stability fluctuation during the rainy season, as an attempt to examine the aspect-dependent landslide initiation by the perspective of classical mechanics and the state of stress (Schmidt et al., 2001). The finite slope model evaluates the stability F_s:

$$F_s = \frac{S_{sr}}{\tau} = \frac{c_l A_l + c_b A_b + A_b(\rho_s - \rho_\omega S_e)\,\mathrm{g}z\cos^2\beta\tan\varphi'}{A_b \rho_s g z \sin\beta\cos\beta} \tag{8}$$

where β is the topographic slope angle, °; A_l is the lateral area, m^2; A_b is the basal area, m^2; z is sliding depth, m; c_l is the sum of the effective soil cohesion and the root additional cohesion along the perimeter, kPa; c_b is the basal soil cohesion, kPa; ρ_s is soil particle density, g/cm^3; ρ_w is water density, g/cm^3.

The infinite slope stability model in this work provides insight into the stress variation resulting from changes in soil suction and water content during infiltration (Lu and Likos, 2006):

$$F_s = \frac{\tan\varphi'}{\tan\beta} + \frac{2c'}{\gamma z\sin 2\beta} - \frac{\sigma^s}{\gamma z}(\tan\beta + \cot\beta)\tan\varphi' \tag{9}$$

where φ' is the effective friction angle, °; β is the topographic slope angle, °; c' is the effective cohesion, kPa; γ is the unit weight of the soil, KN/m^3; σ^s is the suction stress (kPa) and expressed as:

$$\sigma^s = -\frac{S_e}{\alpha}\left(S_e^{n/(1-n)} - 1\right)^{1/n} \tag{10}$$

4 Results

4.1 Shallow landslides on south- and north-facing slope

There were 71 shallow landslides on south-facing slope, while merely 20 landslides on north-facing slope. Figure 2a indicates that the shallow landslides on south-facing slope exhibit larger area than those on north-facing slope. Meanwhile, majority of shallow landslides are on the south-facing slope (Fig. 2b). Furthermore, the volume of landslides on south-facing slope are over those on north-facing slope. For landslides on the south-facing slope, the basal area is 372.64 m^2 and the width is 14.9 m on average. For landslides on north-facing slope, the averaged basal area is merely 157.28 m^2 and the width is 7.7 m (Fig. 2c). Though the landslides on south-facing slope have larger volume and wider width, the depth of head-scar and the sidewall area are no more than the landslides on north-facing slope. Field investigation reveals that the averaged depth for landslides on north-facing slope is 1.02 m, which is deeper than the depth of 0.83 m for landslides on south-facing slope (Fig. 2d). In all, landslides on south-facing slope exhibit overwhelming propensity in number and area, while the failure depth is no more than the landslides on north-facing slope.

Shallow landslides can be modelled as occurring when sufficient through-flow converges from upslope contribution area to hollow area and trigger slope instability (Montgomery and Dietrich, 1994). Their topographic initiation condition is controlled by the spatial competition between slope and upslope contribution area dependent (Stock and Dietrich 2003 and 2006; Horton et al., 2008). For the shallow landslides in the study area, the averaged upslope contributing area and the slope gradient do not differentiate a lot (Fig. 3a), while the lower limit line representing the minimum initiation condition of landslides on south-facing slopes is lower than that on north-facing

https://doi.org/10.5194/egusphere-2022-798
Preprint. Discussion started: 31 August 2022

slope (Fig. 3b). This indicates that higher upslope contributing area is required to provide sufficient through-flow condition and trigger slope failures on north-facing slope. As the landslides in the study area were triggered by the prolonged antecedent precipitation and intensive rainfall (Li et al., 2021), sufficient rainfall infiltration could result in high soil water content within the displaced mass, leading to decrease of the matrix suction and soil strength. The pore pressure generation in response to intense rainfall also plays an important role in shallow landslide. Therefore, we proposed two assumptions to elucidate the aspect-dependent landslide distribution and scale. The first assumption is that the basal area of landslide may relate to the soil strength and the high pore-water pressure. This assumption can be tested by the pore water properties, including the pore water generation potential and dissipation ratio during the failing process. The second assumption is that the south-facing slope may have relatively higher failure potential than the north-facing slope in given rainfall process, which can be elucidated by the stability comparison using the methods of equations (8) and (9).

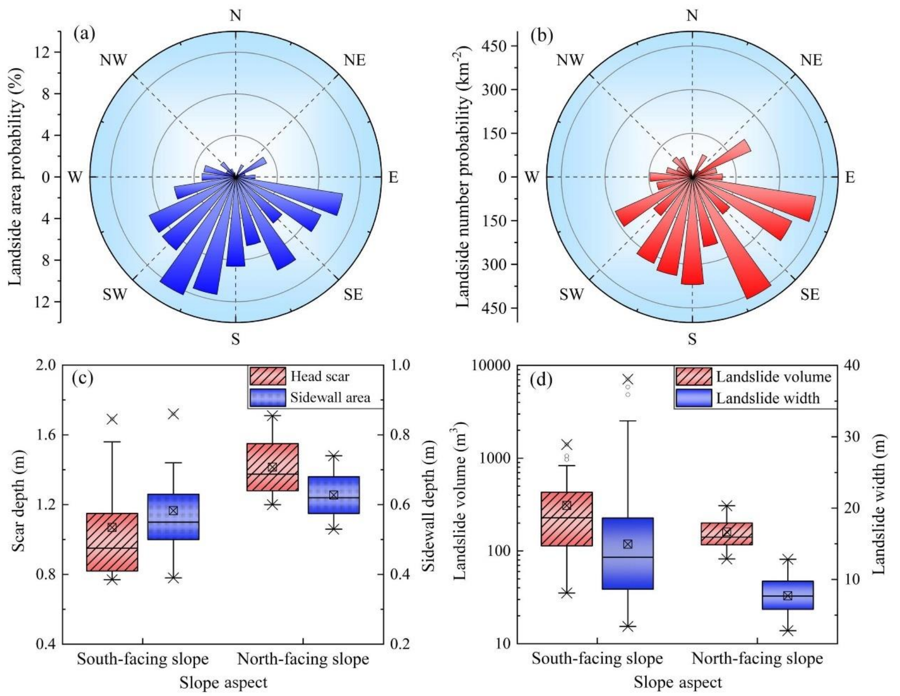

Fig. 2. Spatial distribution and geometric characteristics of landslide: (a) LAP vs slope aspect, (b) LNP vs slope aspect, (c) landslide volume and width vs slope aspect, (d) scar depth and sidewall depth vs slope aspect (the edge line of "box" in the box chart shows the 75th quantile, median and 25th quantile from top to bottom. The length of the box is called the inter-quartile distance. The crossed square inside the box is the average value. The whiskers extend to the maximum and minimum values except outliers. The circle is outliers, and the cross symbol is the maximum and minimum values of all data).

https://doi.org/10.5194/egusphere-2022-798
Preprint. Discussion started: 31 August 2022

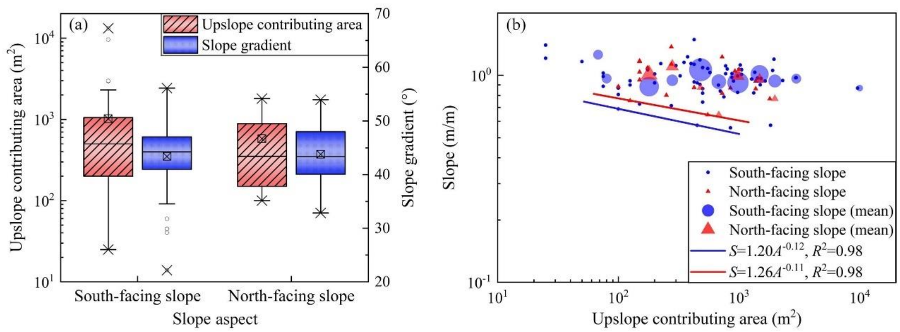

Fig. 3. Upslope contributing area and slope gradient condition: (a) upslope contribution area and mean slope vs slope aspect, (b) the upslope contributing area vs mean slope gradient above landslide area (The large icons are average value with the radius size proportional to the number of landslides. The small icons represent all individual data values).

4.2 Differences in soil physical properties

To reveal the differences in the physical properties of soil mass on both slopes, the dry unit weights, porosity and grain size distribution of soil mass at three layers each slope were firstly compared (Fig. 4). Then, the effective cohesion and inner friction angle were examined with respect to the particle component (Table 1 and fig. 5).

Table 1 Physical properties and strength parameters of soil mass

Parameters	South-facing slope			North-facing slope		
	Layer 1	Layer 2	Layer 3	Layer 1	Layer 2	Layer3
Unit weight of soil (KN/m^3)	14.8	15.6	17.2	14	16.6	17.1
Porosity (%)	43.0	43.1	36.2	42.5	37.3	36.4
Effective cohesion (kPa)	6.5	17.5	21.2	5.3	9.1	7.9
Effective inner friction angle (°)	29.8	25	31	27.1	35.2	41
Saturated hydraulic conductivity (cm/s)	6.4×10^{-3}	6.2×10^{-4}	4.4×10^{-4}	8.8×10^{-3}	1.2×10^{-3}	4.3×10^{-3}

https://doi.org/10.5194/egusphere-2022-798
Preprint. Discussion started: 31 August 2022

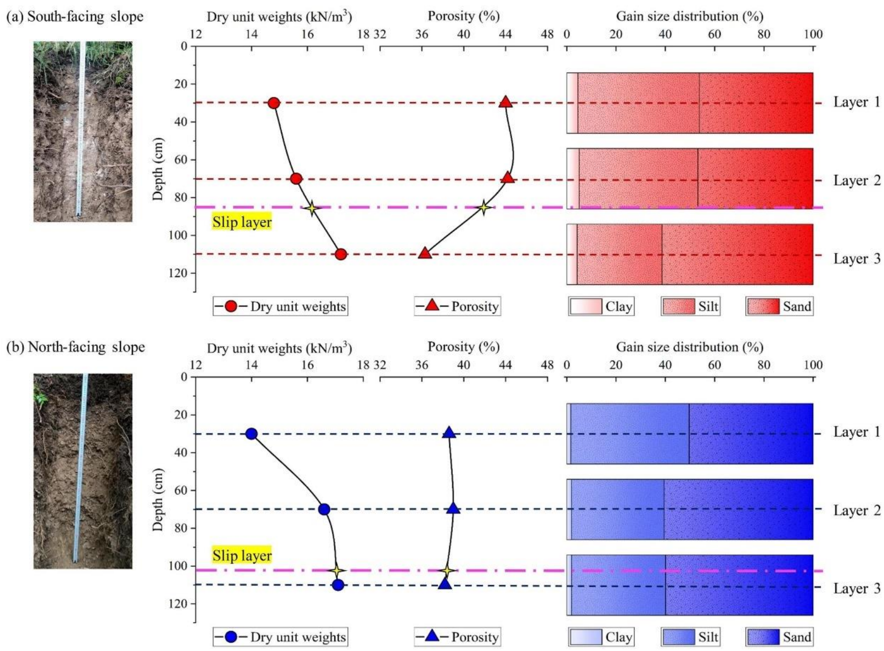

Fig. 4. Differences in the soil properties, including dry unit weights, porosity and grain size in sand, silt, and clay: (a) physical properties of soil mass on the south-facing slope, (b) physical properties of soil mass on the north-facing slope. (The two-soil profile photos were taken by Yanglin Guo during field investigations)

For the soil mass on south-facing slope, the dry unit weights increase as soil depth, while the porosity and saturated hydraulic conductivity decrease (Fig. 4a and table 1). For the soil layers No. 1 and 2, the soil texture is similar as the proportions of sand, silt and clay do not differentiate a lot. However, the proportion of silt at the soil layer No. 3 is no more than the layers No. 1 and 2, and the sand proportion is higher. Besides, the averaged failure depth is above the soil layer No. 3 and is below the layer No. 2. For the soil mass on north-facing slope, the dry unit weights also increase as soil depth. Unlike the south-facing slope, the porosity of soil mass for the three soil layers is about 38% and does not differentiate among them. For the soil texture, the proportion of sand at layer No. 1 is no more than the layers No. 2 and 3 (Fig. 4b). Besides, the depth of failure plane is close to the soil layer No. 3.

In comparison, one of the noticeable differences is the higher saturated hydraulic conductivity for soil mass above the failure plane on south-facing slope, which may result from the high porosity and sand proportion. This indicates that the rainfall infiltration on south-facing slope could penetrate faster than south-facing slope. Indeed, the soil mass of three layers on south-facing slope have relatively higher fine particle proportion than those on north-facing slope, if the gravel is considered (Fig. 5). As noted above, the saturated hydraulic conductivity for soil mass of layers No. 2 and 3 on south-facing slope is lower than that on north-facing slope. This is reasonable because the porosity and proportions of fines on north-facing slope is relatively higher.

https://doi.org/10.5194/egusphere-2022-798
Preprint. Discussion started: 31 August 2022

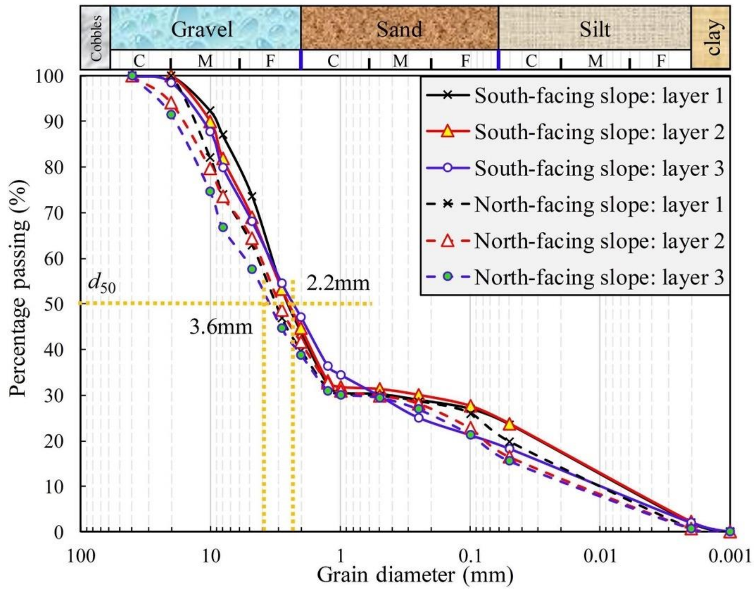

Fig. 5. Soil particle component curves

According to the results of triaxial shear test (Table 1), the soil mass each layer on North-facing slope has smaller effective cohesion comparing to the south-facing slope. In particular, the effective cohesion on the failure plane for landslides on the south-facing slope may be two times of than that on north-facing slope. However, the effective inner friction angles for the soil mass of layers No. 2 and 3 on north-facing slope are far more than those on south-facing slope. Such differences in effective cohesion and inner frictional angle may attribute to the higher clay and silt and less coarse grains within the soil mass on south-facing slope.

4.3 Pore-water pressure property

The consolidation module of triaxial shear test is used to measure the generation and dissipation process of pore water pressure. The principle is to consolidate and drain the soil from the initial saturated state. It is found that under the same confining pressure, there are obvious differences in the consolidation rate, consolidation time and peak rise of pore water pressure of different properties of soil. The results of pore water pressure during the consolidation process under 200kpa effective confining pressure were taken here (Fig. 6). It was found that the peak value of pore water pressure within the soil mass on the south-facing slope was higher than that on the north-facing slope. The peak value of pore water pressure within the soil mass on the south-facing slope could rise to 150~200 kpa. However, the peak value of pore water pressure within the soil mass on the north-facing slope was below 150kPa. Importantly, both of the rising and decaying rate of pore water pressure for soil mass layers No. 1 and 2 on the south-facing slope were lower than that on the north-facing slope. In detail, the rising rate and decaying rate for the soil mass layer No. 2 on the south-facing slope were 1.2kpa/10s and -0.031kpa/10s, respectively. However, they are were 9.6kpa/10s and -0.765kpa/10s for the soil mass on the north-facing slope.

https://doi.org/10.5194/egusphere-2022-798
Preprint. Discussion started: 31 August 2022

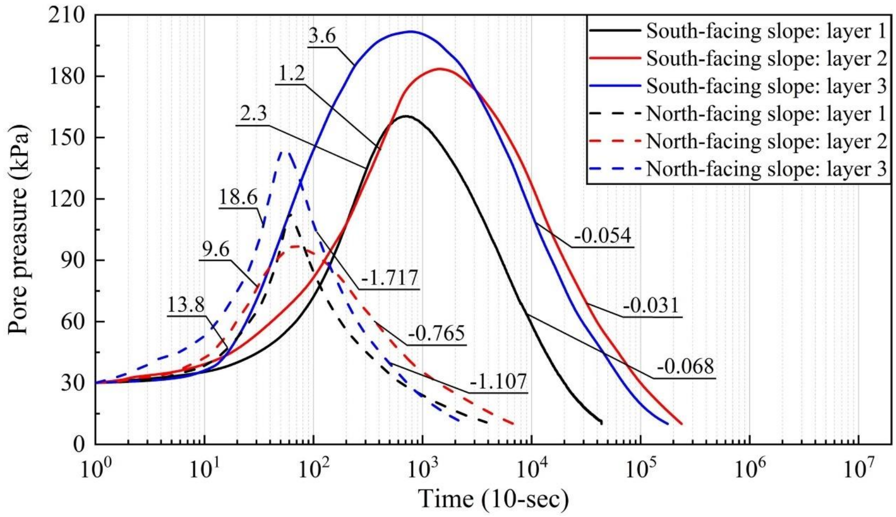

Fig. 6. Variation of pore water pressure under effective confining pressure of 200 kPa by GDS triaxial shear tests.

In fact, the relatively lower peak pore water pressure can illustrate the effect of fine particles on the pore water pressure, which directly affect the landslide mobility and the scale. It is generally believed that the rainfall-induced landslide results from increase of positive pore water pressure within the failure plane, which reduces the effective stress in the soil and the shear strength of the soil (Terzaghi, 1950). This often occurs in the undrained soil layer, which is easy to cause slope liquefaction (Sassa, 1984). The increase of pore water pressure mainly depends on the speed of landslide movement, soil deformation and soil permeability. If the shear rate is the given, the dissipation rate of pore water pressure for high permeability soil is faster, so the increase of pore pressure is smaller (Iverson and LaHusen, 1989; Iverson et al., 1997). As shown in table 1, the saturated hydraulic conductivity for soil mass layers No. 2 and 3 on north-facing slope are commonly 10 times of that on south-facing slope. Therefore, the measured peak pore water pressure during the test for soil mass on south-facing slope would be smaller. Besides, the soil mass on the north-facing slope has relatively higher sand and gravels than that on the south-facing slope (Fig. 5). High clay content on the south-facing slope would fill the macropores within soil mass and reduce the discharge rate of pore water. Wang and Sassa (2003) found that fine particles play the most important role in the dissipation of pore pressure. The pore water pressure within the saturated sand will increase with the shear rate. The soil mass with high coarse particles will produce less pore water pressure than the soil with high fine particles in the shear process. Therefore, high permeability for the soil mass on south-facing slope may result in relatively low peak pore water pressure. The relatively higher fine particles may result in slow rising and dissipation of pore water pressure. Such slow pore water pressure dissipation could result in liquefaction failure of sliding mass and relatively larger landslide area.

4.4 Unsaturated hydraulic conductivity

4.4.1 Measured water outflow mass

Figure 7 shows the measured water outflow mass in given 10 minutes during drying and wetting process. The measured water outflow masses of layers No. 2 and 3 on the north-facing slope are generally higher than those on the south-facing slope. For drying tests using the soil mass of layers No. 2 and 3 on north-facing slope, the given water outflow masses are 0.102g/10-min and 0.131g/10-min respectively. However, the measured water outflow masses are 0.077g/10-min and 0.050g/10-min on south-facing slope, respectively (Fig. 7a). For tests using the same

https://doi.org/10.5194/egusphere-2022-798
Preprint. Discussion started: 31 August 2022

layers of soil mass in wetting process, the measured water outflow masses are 0.051g/10-min and 0.094g/10-min on north-facing slope, respectively, while those are 0.032g/10-min and 0.027g/10-min respectively on south-facing slope (Fig. 7b). As a whole, the permeability of soil mass on the north-facing slope is better than that on the south-facing slope. The same results were also obtained when the saturated hydraulic conductivities of soil layers were measured by the constant water head method (Table 1).

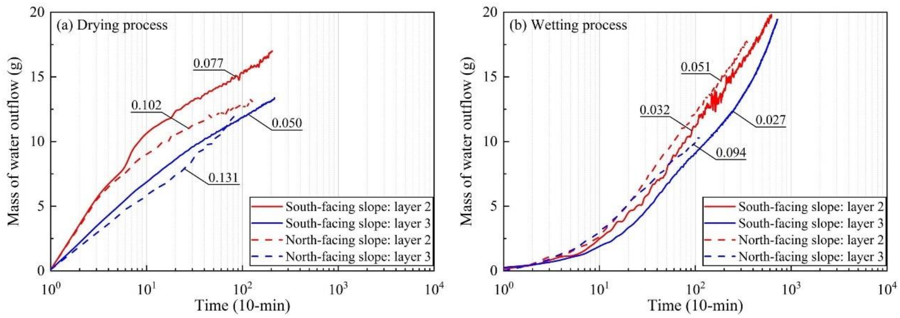

Fig. 7. Mass of water outflow during drying and wetting process: (a) drying tests, (b) wetting tests.

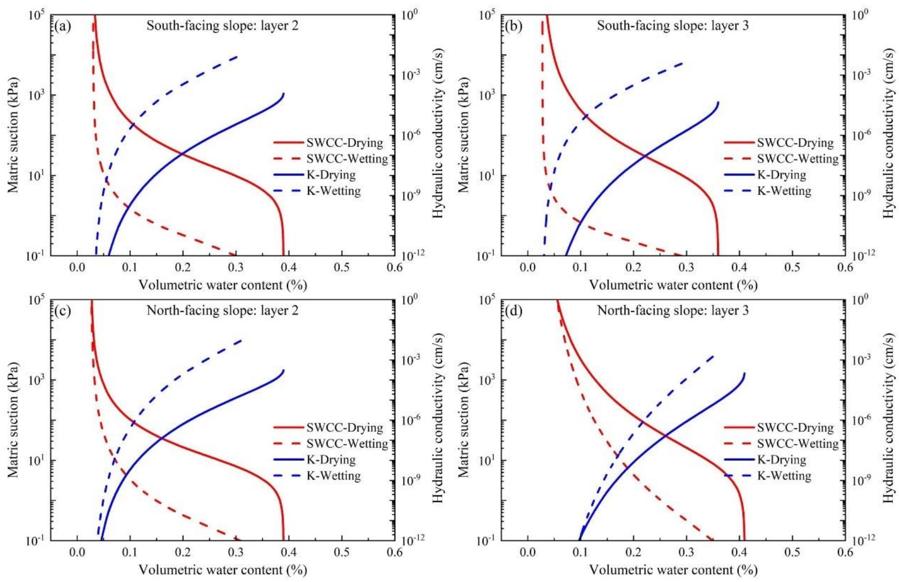

Fig. 8. Soil water characteristic curve obtained by TRIM test: (a) layer No. 2 on south-facing slope, (b) layer No. 3 on south-facing slope, (c) layer No. 2 on north-facing slope, (d) layer No. 3 on north-facing slope.

4.4.2 SWCC and HCF curves

The air-entry pressures and residual water content are two important parameters describing the hydrological and mechanical characteristics of soil. The air-entry pressures represent the critical value when air enters the saturated soil and starts to drain. Table 2 shows the soil characteristic parameters obtained by Hydrus 1-D inversion. Using these parameters, the SWCC and HCF curves of soil mass at soil layer No. 2 and 3 on the north and south-facing slopes can be drawn (Fig. 8). For the soil layer No. 2, the difference between the air-entry values of the north and south-facing slopes can reach 14.03kPa (Figs. 8a and 8c). Besides, the residual water contents and air-entry

https://doi.org/10.5194/egusphere-2022-798
Preprint. Discussion started: 31 August 2022

pressures of the south-facing slope are higher than those of the north-facing slope. For the soil layer No. 3, the soil mass on the north-facing slope has the smallest air-entry pressure, which is 0.51 times of the air-entry pressure of the south-facing slope (Figs. 8b and 8d). The saturated hydraulic conductivities of soil layers No. 2 and 3 on the south-facing slope are lower than those on the north-facing slope in both drying and wetting process. In particular, the saturated hydraulic conductivity of soil mass on the north-facing slope in the wetting test is one order of that on the south-facing slope. These results imply that the soil mass on south-facing slope is more difficult to absorb water and drain water than the soil mass on the north-facing slope.

Table 2 Parameters describing Soil and Water Characteristic Curve (SWCC) and the Hydraulic Conductivity Function (HCF) by Hydrus 1-D

Parameters	South-facing slope		North-facing slope	
	Layer 2	Layer 3	Layer 2	Layer3
θr	0.0302	0.0278	0.0262	0.0268
θs^d	0.39	0.36	0.39	0.41
θs^w	0.36	0.38	0.39	0.42
α^d (kPa^{-1})	0.0128	0.0117	0.0156	0.0141
α^w (kPa^{-1})	0.78	0.94	1.21	1.86
n^d	1.49	1.39	1.57	1.27
n^w	1.63	1.85	1.43	1.18
$K_s{}^d$ (cm/s)	1.52×10^{-4}	0.64×10^{-4}	3.76×10^{-4}	4.56×10^{-4}
$K_s{}^w$ (cm/s)	9.58×10^{-2}	4.93×10^{-2}	4.10×10^{-1}	4.68×10^{-1}
L	0.5	0.5	0.5	0.5

4.5 Water storage and drainage

To exhibit the water storage during the rainfall process and the water drainage after the rainfall, the timely-recorded soil moisture at varied soil layer and the rainfall process during June 11 and August 20 were used (Figs. 9a and 9b). In comparison, the stable soil moisture of layers No. 2 and 3 for both slopes may attribute to long dry seasons in the study area, and the daily rainfall amount > 30 mm on July 9 and 23 resulted in soil moisture increase for all slope layers (Fig. 10a).

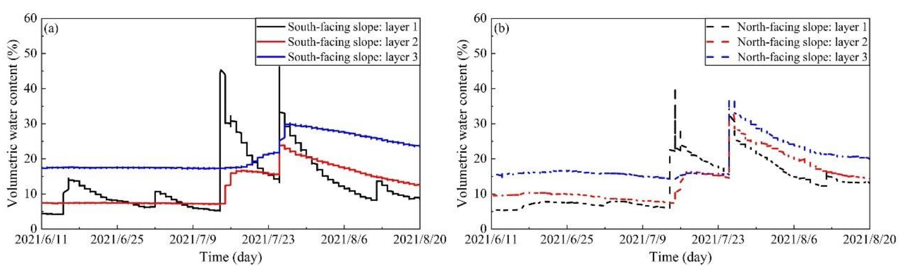

Fig. 9. Field monitored volumetric water content: (a) soil moisture on south-facing slope, (b) soil moisture on north-facing slope.

https://doi.org/10.5194/egusphere-2022-798
Preprint. Discussion started: 31 August 2022

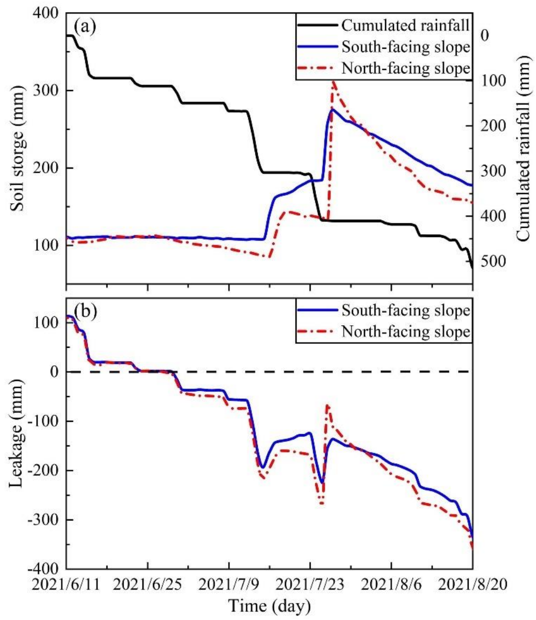

Fig. 10. Seepage model of slope water storage and drainage: (a) soil water storage, (b) soil water drainage

It can be seen from Fig. 10a that the storied water of the north- and south-facing slopes does not synchronously increase with the accumulated precipitation. When the storied water increases rapidly, the increase of the soil water storage of the north-facing slope is larger than that of the south-facing slope. On July 26, a rainfall of 30.8mm/h occurred, and the water storage of the slope reached the peak. It can be seen that the peak of the water storage of the north-facing slope is higher than that of the south-facing slope. However, when the accumulated rainfall tends to be stable, that is, the rainfall stops for a period of time, the decline rate of soil water storage on the north-facing slope is much higher than that on the south-facing slope. In general, the soil water storage of the south-facing slope is always higher than that of the north-facing slope during the rainfall process. In the process of drainage, the seepage rate of the north-facing slope is greater than that of the south-facing slope (Fig. 10b). Therefore, the south-facing slope has better water storage performance and the north-facing slope has higher drainage performance.

4.6 Stability fluctuation

Figure 11a shows the rainfall records from June 11 to August 20, 2021. In general, the saturation degree of the sliding layer of south-facing slope was higher than that on the north-facing slope (Fig. 11b).

In the finite model, the stability of south-facing slope was always higher than that of north-facing slope (Fig. 11c). In the infinite model, the stability of the north-facing slope was generally higher than that of south-facing slope. However, the stability of the north-facing slope fluctuated greatly (Fig. 11d). On July 26, a rainfall event with maximum intensity of 30.8 mm/h resulted in sudden decrease of stability. More importantly, the estimated stability index decreases to be lower than that of the south-facing slope, while increased afterwards. Although the soil moisture of south-facing slope significantly increased in the rainfall event on July 16, the stability fluctuation was so small, which might be related to the relatively strong effective cohesion. It seems that the infinite slope model could better explain the difference of landslide distribution between north and south-facing slope in the study area.

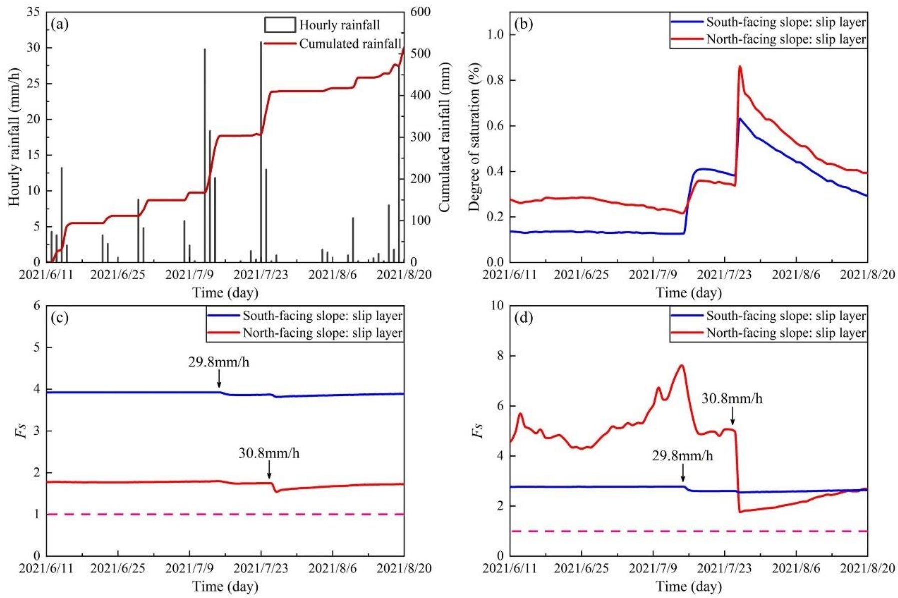

Fig. 11. Change of slope stability fluctuation: (a) rainfall records, (b) degree of saturation, (c) stability of finite slope model, (d) stability of infinite slope model.

5 Discussion

The overwhelming propensity of shallow landslides in some arid or semi-arid mountain region are scientifically interesting and some scholars highlighted the contribution of plant roots. In the Colorado Frontal range, McGuire et al. (2016) found that the apparent cohesion supplied by roots was responsible for the observed connection between landslide distribution and slope aspect (Ebel, 2013; Rengers et al., 2016). Previously, Li et al (2021) found that the plant roots may explain the observed connection between vegetation cover and landslide probability for the whole study area. Then, Dai et al (2022) found that strong root network and high saturated hydraulic conductivity may promote the *A-S* condition of shallow landslide in a localized site near the study area. In the Loess Plateau China, some scholars observed that overwhelming propensity for shallow landslide initiation closely relates to the present-day tree density and the failure depth would increase as the plant roots (Guo et al., 2020; Deng et al., 2022). However, the overwhelming propensity of shallow landslides on north- and south-facing slope couldn't attribute to the plant roots as the man-made vegetation on both slopes are same.

This work contributes to know about the aspect-dependent landslide initiation by the perspective of soil hydraulic properties, other from the mechanical and hydrological effects of plant roots. Except the overwhelming propensity, the shallow landslides on south-facing slope exhibit relatively larger area and wider width than those on north-facing slope (Fig. 2). In comparison, the effective cohesion of failure zone on south-facing slope is stronger than that on north-facing slope. It seems that the basal area of shallow landslide in the study area may attribute to the effective cohesion as some statistical results reveal that incoherent materials favor shallow landslides with no limitation in size; while cohesive materials favor deep landslides and show a limitation for small sizes (Larsen et al., 2010; Frattini and Crosta, 2013; Milledge et al., 2014). However, stronger effective cohesion tends to promote the *A-S* condition of shallow landslides. In other words, a relatively larger up-slope contributing area or steeper gradient is required to trigger slope failures. In fact, fig. 3 illustrate that some shallow landslides on south-facing slope fail on relatively lower upslope contributing area. Therefore, the soil hydraulic properties-related factors, such as the rising or dissipation of pore water pressure, water storage and drainage may contribute to the observed phenomena.

The saturated hydraulic conductivities by variable-head permeameter and TRIM methods coincide with each other, which together prove that the soil mass on north-facing slope has a relatively larger water infiltration (Tables 1 and 2). However, the results of stability analysis by the finite and infinite models imply that the failure potential of slides on north-facing slope is relatively lower than the south-facing slope, though the stability index fluctuate more heavily than north-facing slope. Such differences imply slope failures on north-facing slope may occur on condition of intensive rainfall merely, or by a combination of prolonged antecedent precipitation and short-duration intensive rainfall. For potential failures on south-facing slope, the combination of prolonged antecedent precipitation and short-duration intensive rainfall should be the possible trigger due to the low hydraulic conductivity and pore water pressure dissipation. Additionally, this work mainly concerns on the hydraulic properties of the soil mass on both slopes. The origins of the soil mass on both slopes (particularly the soil mass on the failure zone), either from the weathered granite underneath or the Loess deposits, needs further investigation in future. Last but not least, this work contributes to propose a different opinion on the observed connection between landslide distribution and slope aspect from the perspective of soil hydraulic properties.

6 Conclusion

Previous researches about the overwhelming propensity shallow landslides on south-facing slope over north-facing slope highlighted the role of plant roots. In a localized area with same vegetation, such observation couldn't attribute to plant roots and may result from soil hydraulic properties-related factors. In this work, we present a study on the aspect-dependent landslide initiation by the perspective of pore water pressure, unsaturated hydraulic conductivity, water storage and drainage and the hillslope stability fluctuation during the monitoring duration. The following conclusions can be drawn:

(1) In terms of soil physical and mechanical properties on both slopes, the soil masses on south-facing slope are rich in clay content, while the soil mass on north-facing slope has high sand. The effective cohesion on soil mass on south-facing slope is higher than that on north-facing slope, while the effective frictional angle is smaller.

(2) Results of the GDS tests reveal that the dissipation rate of pore water pressure for soil mass on the south-facing slope is much lower than that in the north-facing slope. Higher effective cohesion and the slower pore water pressure dissipation may result in the larger basal area of shallow landslides on south-facing slope.

(3) The soil mass on south-facing slope has higher residual water content and air-entry pressure, and lower saturated hydraulic conductivity than that on the north-facing slope. For the water storage and drainage performance, the storied water of the south-facing slope is higher than that of the north-facing slope, while the north-facing slope has a higher leakage rate. Results of the stability analysis on basis of finite and infinite model illustrate that the infinite slope model may be suitable for elucidating the aspect-dependent landslide distribution in the study area.

Acknowledgements

This study was supported by the Fundamental Research Funds for the Central Universities (Grant No. 2018BLCB03), State Key Program of National Natural Science of China (Grant No. 42130701), and the National Nature Science Foundation of China (42177309). The authors sincerely thank the contribution from other colleges, including Muyang Li, Zhisheng Dai, Lv Miao, Lijuan Wang, Jiayong Deng, for the previous work near the study area.

Code/Data availability

The raw/processed data in this work cannot be shared at this time as the data also forms part of an ongoing study

Author contribution

Professor Ma Chao found the overwhelming propensity of shallow landslide initiation on south-facing hillslope in the study area and launched the research proposal. Miss Yanglin Guo finished the sampling collection and indoor tests.

Competing interests

All authors have declared that there were no conflicts of interests and competing interests.

References

[1] Alessio, P.: Spatial variability of saturated hydraulic conductivity and measurement-based intensity-duration thresholds for slope stability, Santa Ynez Valley, CA, Geomorphology, 342, 103-116, https://doi.org/10.1016/j.geomorph.2019.06.004, 2019.

[2] Bogaard, T. A., Greco, R.: Landslide hydrology: from hydrology to pore pressure, Wiley Interdiscip. Rev. Water, 3, 439-459, https://doi.org/10.1002/wat2.1126, 2016.

[3] Brenner, R. P., Tam, H. K., Brand, E. W.: Field stress path simulation of rain-induced slope failure, Proceedings of 11th International Conference on Soil Mechanics and Foundation Engineering, vol. 2, pp. 373-376, 1985.

[4] Coe, J. A., Kean, J. W., Godt, J. W., Baum, R. L., Jones, E. S., Gochis, D. J., Anderson, G. S.: New insights into debris-flow hazards from an extraordinary event in the Colorado front range, GSA Today, 24, 4-10, https://doi.org/10.1130/GSATG214A.1, 2014.

[5] Dai, Z. S., Ma, C., Miao, L., Li, M. Y., Wu, J. L. and Wang, X. H.: Initiation conditions of shallow landslides in two man-made forests and back estimation of the possible rainfall threshold, Landslides, 19, 1031-1044, https://doi.org/10.1007/s10346-021-01823-1, 2022.

[6] Deng, J. Y., Ma, C., and Zhang, Y.: Shallow landslide characteristics and its response to vegetation by example of July 2013, extreme rainstorm, Central Loess Plateau, China. Bulletin of Engineering Geology and the Environment, 81-100, https://doi.org/10.1007/s10064-022-02606-1, 2022.

[7] Ebel, B. A.: Wildfire and aspect effects on hydrologic states after the 2010 Fourmile canyon fire, Vadose Zone, 12, 1-19, http://doi.org/10.2136/vzj2012.0089, 2013.

[8] Ebel, B. A., Rengers, F. K., Tucker, G. E.: Aspect-dependent soil saturation and insight into debris-flow initiation during extreme rainfall in the Colorado front range, Geology, 43, 659-662, https://doi.org/10.1130/G36741.1, 2015.

[9] Frattini, P., Crosta, G. B.: The role of material properties and landscape morphology on landslide size distributions, Earth Planet. Sci. Lett., 361, 310-319, https://doi.org/10.1016/j.epsl.2012.10.029, 2013.

[10] Fredlund, D. G., Morgenstern, N. R., Widger, R. A.: The shear strength of unsaturated soils, Can. Geotech. J., 15, 313-321, https://doi.org/10.1139/t78-029, 1978.

[11] Fredlund, D. G., Xing, A., Fredlund, M. D., Barbour, S. L.: The relationship of the unsaturated soil shear strength to the soil-water characteristic curve, Can. Geotech. J., 33, 440-448, https://doi.org/10.1139/t96-065, 1996.

[12] Fredlund, D. G., Xing, A., Huang, S.: Predicting the permeability function for unsaturated soils using the soil-water characteristic curve, Can. Geotech. J., 31, 521-532, https://doi.org/10.1139/t94-062, 1994.

[13] Fu, B. J., Wang, Y. F., Lu, Y. H., He, C. S., Chen, L. D., Song, C. J.: The effects of land-use combinations on soil erosion: a case study in the Loess Plateau of China, Prog. Phys. Geo., 33, 793-804, https://doi.org/10.1177/0309133309350264, 2009.

[14] Geroy, I. J., Gribb, M. M., Marshall, H. P., Chandler, D. G., Benner, S. G., McNamara, J. P.: Aspect influences on soil water retention and storage, Hydrol. Processes, 25, 3836-3842, https://doi.org/10.1002/hyp.8281, 2011.

[15] Godt, J. W., Baum, R. L., and Lu, N.: Landsliding in partially saturated materials. Geophys. Res. Lett., 36, L02403, https://doi.org/10.1029/2008GL035996, 2009.

[16] Guo, F. Y., Meng, X. Y., Li, Z. H., Xie, Z. T., Chen, G., He, Y. F.: Characteristics and causes of assembled geo-hazards induced by the rainstorm on 25th July 2013 in Tianshui City, Gansu, China, Mt. Res., 33, 100-107, 2015 (in Chinese)

[17] Guo, W. Z., Chen, Z. X., Wang, W. L., Gao, W. W., Guo, M. M., Kang, H. L., Li, P. F., Wang, W. X., Zhao, M.: Telling a different story: The promote role of vegetation in the initiation of shallow landslides during rainfall on the Chinese Loess Plateau, Geomorphology, 350, 106879, https://doi.org/10.1016/j.geomorph.2019.106879, 2020.

[18] Iverson, R. M., LaHusen, R. G.: Dynamic pore-pressure fluctuations in rapidly shearing granular materials, Science, 246, 796-799, https://doi.org/10.1126/science.246.4931.796, 1989.

[19] Iverson, R. M., Reid, M. E., LaHusen, R. G.: Debris-flow mobilization from landslides, Annu. Rev. Earth Planet. Sci., 25, 85-138, https://doi.org/10.1146/annurev.earth.25.1.85, 1997.

[20] Lan, H. X., Zhou, C. H., Lee, C. F., Wang, S. J., Wu, F. Q.: Rainfall-induced landslide stability analysis in response to transient pore pressure-A case study of natural terrain landslide in Hong Kong, Science in China Ser. E Technological Sciences, 46, 52-68, 2003.

[21] Larsen, I. J., Montgomery, D. R., Korup, O.: Landslide erosion controlled by hillslope material, Nat. Geosci., 3, 247-251, https://doi.org/10.1038/ngeo776, 2010.

[22] Lee, E., Kim, S. Seasonal and spatial characterization of soil moisture and soil water tension in a steep hillslope, J. Hydrol., 568, 676-685, https://doi.org/10.1016/j.jhydrol.2018.11.027, 2019.

[23] Li, C. S., Kong, L. W., Bai, W., An, R., Li, T. G.: Hysteresis model of soil-water characteristic curve, Rock and Soil Mechanics, 39, 598-604, 2018 (in Chinese)

[24] Li, M. Y., Ma, C., Du, C., Yang, W. T., Lyu, L. Q., Wang, X. H.: Landslide response to vegetation by example of July 25-26, 2013, extreme rainstorm, Tianshui, Gansu Province, China, Bull. Eng. Geol. Environ., 80, 751-764, https://doi.org/10.1016/10.1007/s10064-020-02000-9, 2021.

[25] Long, H.: Research on the mechanism of pore water action within unsaturated soil and the corresponding slope stability, Chongqing University, 2012 (in Chinese)

[26] Lu, N., and Godt. J. W.: Hillslope hydrology and stability, Cambridge Univ. Press, Cambridge, UK, 2013.

[27] Lu, N., and Likos, W. J.: Unsaturated Soil Mechanics, John Wiley & Sons, New York, 2004.

[28] Lu, N., and Likos, W. J.: Suction stress characteristic of unsaturated soils, J. Geotech. Geoenviron. Eng., 132, 131-142, http://doi.org/10.1061/(ASCE)1090-0241(2006)132:2(131), 2006.

[29] Lu, N., Godt, J. W.: Infinite slope stability under steady unsaturated seepage conditions, Water Resour. Res., 44, W11404, https://doi.org/10.1029/2008WR006976, 2008.

[30] Marino, P., Santonastaso, G. F., Fan, X., Greco, R.: Prediction of shallow landslides in pyroclastic-covered slopes by coupled modeling of unsaturated and saturated groundwater flow, Landslides, 18, 31-41, https://doi.org/10.1007/s10346-020-01484-6, 2021.

[31] McGuire, L. A., Rengers, F. K., Kean, J. W., Coe, J. A., Mirus, B. B., Baum, R. L., Godt, J. W.: Elucidating the role of vegetation in the initiation of rainfall-induced shallow landslides: insights from an extreme rainfall event in the Colorado front range, Geophys. Res. Lett., 43, 9084-9092, https://doi.org/10.1002/2016GL070741, 2016.

[32] Milledge, D. G., Bellugi, D., McKean, J. A., Densmore, A. L., Dietrich, W. E.: A multidimensional stability model for predicting shallow landslide size and shape across landscapes, J. Geophys. Res.: Earth Surf., 119, 2481-2504, https://doi.org/10.1002/2014JF003135, 2014.

[33] Montgomery, D. R., Dietrich, W. E.: Landscape dissection and drainage area-slope thresholds, In: Kirkby MJ (ed) Process models and theoretical geomorphology, John Wiley, Hoboken, N. J., pp: 221-246, 1994.

[34] Morgenstern, N. R., and de Matos, M. M.: Stability of slopes in residual soils, in Proceedings of the 5th Panamerican Conference on Soil Mechanics and Foundation Engineering, Buenos Aires, 3, 367-383, 1975.

[35] Mualem, Y.: Hysteretical models for prediction of the hydraulic conductivity of unsaturated porous media, Water Resour. Res., 12, 1248-1254, https://doi.org/10.1029/WR012i006p01248, 1976.

[36] Qiu, H. J., Cui, Y. F., Hu, S., Yang, D.D., Pei, Y. Q. and Yang, W. L.: Temporal and spatial distributions of landslides in the Qinba Mountains, Shaanxi Province, China, Geomatics, Natural Hazards and Risk, 10, 599-621, https://doi.org/10.1080/19475705.2018.1536080, 2019.

[37] Reid, M. E., LaHusen, R. G., Iverson, R. M.: Debris-flow initiation experiments using diverse hydrologic triggers, Debris-Flow Hazards Mitigation: Mechanics, Prediction and Assessment, edited by C. L. Chen, pp. 1-10, American Society of Civil Engineering, New York, 1997.

[38] Rengers, F. K., McGuire, L. A., Coe, J. A., Kean, J. W., Baum, R. L., Staley, D. M., Godt, J. W.: The influence of vegetation on debris-flow initiation during extreme rainfall in the northern Colorado front range, Geology, 44, 823-826, http://doi.org/10.1130/G38096.1, 2016.

[39] Sassa, K.: The mechanism starting liquefied landslides and debris flows. Proceedings of 4th International Symposium on Landslides, Toronto, Canada, vol. 2, pp. 349-354, 1984.

[40] Schmidt, K. M., Roering, J. J., Stock, J. D., Dietrich, W. E., Montgomery, D. R., Schaub, T.: The variability of root cohesion as an influence on shallow landslide susceptibility in the Oregon Coast Range, Can. Geotech., 38, 995-1024, 2001.

[41] Sidle, R., Ochiai, H.: Landslides: Processes, prediction, and land use, Water Resour. Monogr. Ser. 18, AGU, Washington DC, https://doi.org/10.1029/WM018, 2006.

[42] Smith, T. J., McNamara, J. P., Flores, A. N., Gribb, M. M., Aishlin, P. S., Benner, S. G.: Small soil storage capacity limits benefit of winter snowpack to upland vegetation, Hydrol. Processes, 25, 3858-3865, https://doi.org/10.1002/hyp.8340, 2011.

[43] Terzaghi, K.: Mechanism of landslides. In: Paige, S. (Ed.), Application of Geology to Engineering Practice (Berkey Volume). Geological Society of America, New York, pp. 83-123, 1950.

[44] Thomas, M. A., Mirus, B. B., Collins, B. D., Lu, N. and Godt, J. W.: Variability in soil-water retention properties and implications for physics-based simulation of landslide early warning criteria, Landslides, 15, 1265-1277, https://doi.org/10.1007/s10346-018-0950-z, 2018.

[45] Timilsina, S., Niemann, J. D., Rathburn, S. L., Rengers, F. K., Nelson, P. A.: Modeling hydrologic processes associated with soil saturation and debris flow initiation during the September 2013 storm, Colorado Front Range, Landslides, 18, 1741-1759, https://doi.org/10.1007/s10346-020-01582-5, 2021.

[46] Trustrum, N. A., Gomez, B., Page, M. J., Reid, L. M. and Hicks, D. M.: Sediment production, storage and output: The relative role of large magnitude events in steepland catchments, Zeitscrift für Geomorphologie Supplement Band, 115, 71-86, https://doi.org/10.1127/zfgsuppl/115/1999/71, 1999.

[47] Van Genuchten, M. T.: A closed-form equation for predicting the hydraulic conductivity of unsaturated soils, Soil Sci. Soc. Am. J, 44, 892-898, https://doi.org/10.2136/sssaj1980.03615995004400050002x, 1980.

[48] Wang, C. Y.: Study on the relationship between aspect and slope stability, Dissertation, Kunming University of Science and Technology, 2008 (in Chinese).

[49] Wang, G. H., Sassa, K.: Pore-pressure generation and movement of rainfall-induced landslides: effects of grain size and fine-particle content, Eng. Geol., 69, 109-125, https://doi.org/10.1016/S0013-7952(02)00268-5, 2003.

[50] Wang, G., Sassa, K., Fukuoka, H.: Downslope volume enlargement of a debris slide-debris flow in the 1999 Hiroshima, Japan, rainstorm. Eng. Geol., 69, 309-330, https://doi.org/10.1016/S0013-7952(02)00289-2, 2003.

[51] Wang, X. H., Ma, C., Wang, Y. Q., Wang, Y. J., Li, T., Dai, Z. S., Li, M. Y.: Effect of root architecture on rainfall threshold for slope stability: variabilities in saturated hydraulic conductivity and strength of root-soil composite, Landslides, 17, 1965-1977, https://doi.org/10.1007/s10346-020-01422-6, 2020.

[52] Wayllace, A., Lu, N.: A transient water release and imbibitions method for rapidly measuring wetting and drying soil water retention and hydraulic conductivity functions. Geotech. Test. J., 35, 1-15, 2012.

[53] Wieczorek, G. F., Glade, T.: Climatic factors influencing the occurrence of debris flows, in: Hungr, O. and Jacob, M. eds., Debris flow hazards and related phenomena: Praxis, Springer, Berlin, Heidelberg, 325-362, https://doi.org/10.1007/3-540-27129-5_14, 2005.

[54] Xia, D., Deng, Y. S., Wang, S. L., Ding, S.W., Cai, C.F.: Fractal features of soil particle-size distribution of different weathering profiles of the collapsing gullies in the hilly granitic region, south China. Natural Hazards, 79, 455-478, https://doi.org/10.1007/s11069-015-1852-1, 2015.

[55] Xia, J. W., Cai, C. F., Wei, Y. J., Wu, X. L.: Granite residual soil properties in collapsing gullies of south China: spatial variations and effects on collapsing gully erosion, Catena, 174, 469-477, https://doi.org/10.1016/j.catena.2018.11.015, 2019.

[56] Yang, Z. J., Qiao, J. P., Uchimura, T., Wang, L., Lei, X. Q., Huang, D.: Unsaturated hydro-mechanical behavior of rainfall-induced mass remobilization in post-earthquake landslides, Eng. Geol., 222, 102-110, https://doi.org/10.1016/j.enggeo.2017.04.001, 2017.

[57] Youd, T.L., Gilstrap, S.G.: Liquefaction and deformation of silty and fine-grained soils. Proceedings of 2nd International Conference on Earthquake Geotechnical Engineering, Lisbon, Portugal, vol. 3, pp. 1013-1020, 1999.

[58] Yu, G. Q., Zhang, M. S., Hu, W.: Analysis on the development characteristics and hydrodynamic conditions for massive debris flow in Tianshui, Northwest Geol., 47, 185-191, 2014 (in Chinese)

[59] Zhou, Z. C., Shangguan, Z. P., Zhao, D.: Modeling vegetation coverage and soil erosion in the Loess Plateau Area of China. Ecol. Modell., 198, 263-268, https://doi.org/10.1016/j.ecolmodel.2006.04.019, 2006.

[60] Zuo, R., Agterberg, F. P., Cheng, Q., Yao, L.: Fractal characterization of the spatial distribution of geological point processes, International Journal of Applied Earth Observation and Geoinformation, 11, 394-402, https://doi.org/10.1016/j.jag.2009.07.001, 2009.